Int. J. Electrochem. Sci., 13 **(2018)** 12163 – 12171, doi: 10.20964/2018.12.20

International Journal of ELECTROCHEMICAL SCIENCE
www.electrochemsci.org

Electrochemical Corrosion Study of Zircaloy-4 in a LiOH Solution at High Temperature and Pressure

Zhuo Wang[1, 2], *Heping Li*[1*], *Liping Xu*[1], *Qingyou Liu*[1], *Lei Zha*[1, 2], *Sen Lin*[1]

[1] Key Laboratory of High Temperature and High Pressure Study of the Earth's Interior, Institute of Geochemistry, Chinese Academy of Sciences, Guiyang, China
[2] University of Chinese Academy of Sciences, Beijing, 100039, China
[*]E-mail: liheping@vip.gyig.ac.cn

Received: 27 July 2018 / *Accepted:* 21 September 2018 / *Published:* 5 November 2018

The electrochemical corrosion of Zircaloy-4 in simulated pressurized water reactor coolant at 350°C was studied via in situ potentiodynamic polarization and electrochemical impedance spectroscopy (EIS) measurements. The potentiodynamic polarization results indicate that the corrosion potential of Zircaloy-4 decreases and its corrosion current density increases when the concentration of LiOH increases, showing that Zircaloy-4 corrodes more easily and faster in higher concentrations of LiOH. In addition, the EIS data fits the double layer oxide model, which consists of a porous non-protective outer layer and a dense protective inner barrier layer. The EIS data suggest that the corrosion resistance of the two oxide layers both decrease with the increasing LiOH concentration. Our study shows that increasing the LiOH concentration benefits the electrochemical corrosion of Zircaloy-4 in high-temperature and high-pressure aqueous solutions.

Keywords: Zircaloy-4; EIS; polarization; corrosion; oxidation; Modeling and Simulation

1. INTRODUCTION

Zirconium alloys, which have good corrosion resistance, considerable operational performance, sufficient mechanical properties and a low absorption cross section of thermal-spectrum neutrons in high-temperature and high-pressure aqueous environments, have been widely applied to the fuel cladding and structural materials of nuclear reactors [1-3]. However, the corrosion of zirconium alloys in severe environments is a critical factor that affects their service life and, consequently, ~~for~~ nuclear security and radiation safety [4-5]. It has been reported that zirconium alloys with different chemical compositions are suited for different applications. For example, the Zr-Sn alloy has been used as fuel cladding for many years, and Zircaloy-2 and Zircaloy-4 are usually used as ~~the~~ structural materials in a boiling water reactor (BWR) and a pressurized water reactor (PWR) [3-5], respectively.

In most published studies, researchers [6-13] have tended to study the corrosion behavior of zirconium alloys by measuring weight gain and ~~by~~ using surface analysis methods such as transmission electron microscope (TEM), scanning electron microscope (SEM) and X-ray diffraction (XRD), which only consider~~s~~ the influence of chemical corrosion on the zirconium alloys. Several investigations [14-19] have used EIS to analyze the structure of the oxide film formed on zirconium alloys, but these data were measured at room temperature after exposure of the alloys in a static autoclave, which does not illustrate the actual performance of zirconium alloys in a high-temperature and high-pressure aqueous solution. In recent studies, EIS has been applied in situ. Ai et al. [20, 21] developed an impedance model based on the Point Defect Model to estimate the thickness of the oxide layer formed on zirconium alloys under simulated PWR coolant conditions at 250°C and 62 bar~~, while~~ Bojinov et al. [22, 23] studied the thickness of the oxide layer on Zircaloy-2 in a simulated BWR and WWER environment by an impedance model based on the Mixed Conduction Model.

In most PWRs, LiOH has been added to the primary coolant system to maintain the pH of the reaction environment in order to control the transport of the products [24]. Liu et al. [25] found Li^+ and OH^- by second ion mass spectrometry (SIMS) in the zirconium oxide film when the alloy was exposed to a LiOH aqueous solution. Müller [26] reported that the corrosion rates of Zircaloy-4, Zircaloy-2.5Nb and Zr-1Nb increased when the concentration of LiOH was above 0.1 M at 343°C by measuring the weight gain and ~~by~~ XRD analysis. However, the concentrations of LiOH used in this study were much higher than the actual amount of LiOH in the PWR system. Bojinov et al. [27] studied the oxidation of E110, one of the Zr-Nb alloys, under simulated light water reactor (LWR) conditions at 310°C by using in situ EIS and the Mixed Conduction Model to estimate the thickness of the zirconium oxide film in 2.2, 5.4, 10 ppm LiOH solutions, which approximately equal~~s~~ the theoretical concentration of LiOH in conventional PWRs. However, Palmer et al. [28] reported that Li^+ and OH^- ions were adsorbed on the zirconium oxide surface at 350°C and 360°C, leading to the possibility that the LiOH concentration could be increased. Although there is a circulating water system in nuclear reactors, the LiOH has the potential to remain in the pores or cracks formed on the zirconium oxide film due to ~~the~~ corrosion, creating a larger concentration of LiOH in ~~the~~ zirconium alloys in the service environment. This study considers the extreme LiOH concentrations that are theoretically possible. In this work, the electrochemical corrosion behavior of Zircaloy-4, a common Zr-Sn alloy, was studied by in situ potentiodynamic polarization and EIS measurements under simulated PWR coolant situation at 350°C and 16.5 MPa in solutions with LiOH concentrations ranging from 10 ppm to 10^4 ppm. The aim of this work is to understand the characteristics of the zirconium oxide film formed on the Zircaloy-4 surface and the influence of LiOH on the anticorrosive ability of Zircaloy-4 in extreme simulated nuclear reactor environments.

2. EXPERIMENTAL

The Zircaloy-4 sample used in this study contained 1.3% Sn, 0.2% Fe, 0.1% Cr, and balanced Zr. The sample was shaped into a cone frustum with an exposed working area of 0.47 cm^2. Prior to electrochemical measurements, the zirconium alloy electrode was sequentially polished with 1500,

2500, and 3000-grit SiC paper to obtain a fresh surface and then washed with alcohol, acetone and deionized water. The electrolyte was a LiOH solution at concentrations of 10, 10^2, 10^3, and 10^4 ppm prepared with deionized water and analytical pure LiOH. Analytical grade LiOH and double distilled water were used to prepare a series of LiOH solutions of various concentrations. During all experiments, the electrochemical reaction autoclave was equipped with 18 mL of a LiOH solution.

Electrochemical measurements were performed using a computer-controlled electrochemical measurement system (PARSTAT 2263, Princeton Applied Research) with a conventional three-electrode electrolytic cell in a self-designed autoclave. In this three-electrode system, the working electrode was the zirconium alloy electrode, which was sealed and electrically insulated from the autoclave with a 1 mm thick pyrophyllite taper sleeve. The counter electrode was a self-designed platinum electrode that was made of an alumina ceramic cone frustum with a platinum wire in its central axis. To achieve a sufficient counter electrode surface area, a platinum power was sintered onto its end surface. The and the reference electrode was an Ag/AgCl pressure-balanced external electrode filled with 0.1 M KCl. In the present work, the measured potential can be normalized with respect to the saturated hydrogen electrode (SHE) using the following formula [29]:

$$\Delta E_{\mathrm{SHE}} = \Delta E_{\mathrm{obs}} + 286.6 - \Delta\mathrm{T} + 1.745 \times 10^{-4}\Delta\mathrm{T}^2 - 3.03 \times 10^{-6}\Delta\mathrm{T}^3 \ (\mathrm{mV})$$

All of the other potentials in this study are quoted relative to the Ag/AgCl electrode unless otherwise stated. The details of the experimental apparatus can be found in another paper published by our group [30]. The experiments were conducted at 350°C (± 0.5°C) and 16.5 MPa (± 0.3 MPa). We used a resistance furnace to heat the autoclave, which was made of titanium alloy. The temperature was controlled by a temperature controller, and the measuring junction of the thermocouple was placed near the Zircaloy-4 sample. The pressure in the system was measured by a pressure sensor.

Potentiodynamic measurements were made at a scan rate of 1 $mV \cdot s^{-1}$ and a range from -0.7 V to 2.4 V relative to the open current potential (OCP). EIS tests were performed with an amplitude of 10 mV in the frequency range from 0.01 Hz to 10000 Hz after OCP stabilization, and ZSimpWin software was used to fit the impedance data.

3. RESULTS AND DISCUSSION

3.1. Potentiodynamic measurement

Figure 1 illustrates the potentiodynamic polarization behavior of Zircaloy-4 in an aqueous solution with different concentrations of LiOH at 350°C and 16.5 MPa. These curves showed similar E-I profiles, where the current density increases slowly at the anodic polarization branch until approximately 1.6 V. The growth and dissolution of zirconium oxide directly affects the corrosion behavior of Zircaloy-4. It is obvious that the curves show a passive region, which extends to approximately 1.6 V, resulting from the formation of a passive oxide film on the zirconium alloy. Therefore, Zircaloy-4 has ~~a~~ good corrosion resistance in LiOH solutions at high-temperature and high-pressure due to the wide anodic passive region. Table 1 lists the results of the Tafel region extrapolations from the polarization experiments.

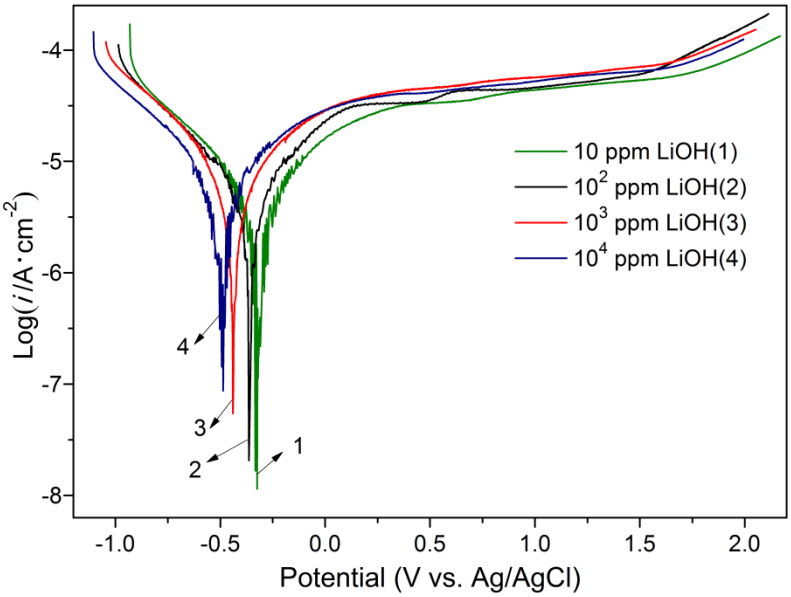

Figure 1. Polarization curves of Zircaloy-4 in LiOH solutions with different concentrations (350°C, 16.5 MPa)

Table 1. Polarization parameters of Zircaloy-4 in LiOH solution with different concentrations (350°C, 16.5 MPa)

C_{LiOH} (ppm)	E_{corr} (mV)	i_{corr} (μA·cm^{-2})	β_a (mV·dec^{-1})	β_c (mV·dec^{-1})
10	-317.5	0.389	431.1	154.2
10^2	-362.6	3.56	385.1	193.1
10^3	-438.8	6.17	278.5	246.6
10^4	-492.6	6.34	235.2	306.8

As the concentration of LiOH increases from 10 to 10^4 ppm, the corrosion potential (E_{corr}) decreases from -317.5 mV to -492.6 mV and the corrosion current density (i_{corr}) increases from 0.389 μA·cm^{-2} to 6.34 μA·cm^{-2}. These changes indicate that Zircaloy-4 corrodes easier and faster when the concentration of LiOH increases. In addition, the pitting corrosion that occurs at approximately 1.6 V is almost unchanged with the increasing LiOH concentration, which shows that LiOH has little influence on the pitting corrosion resistance of Zircaloy-4. A possible explanation of the observation above is that the addition of LiOH facilitates the dissolution of zirconium oxide at its interface with the electrolyte. The main reactions of the zirconium oxide are shown as follows [27, 31]:

Anode reaction: $$Zr \rightarrow Zr^{4+} + 4e^- \quad (1)$$

Cathode reaction: $$2H_2O + 4e^- \rightarrow 2O_o + 4H_{bl} \quad (2)$$

$$ZrO_2 + OH^- \rightarrow HZrO_3^- \quad (3)$$

Reaction (1) mainly contributes to the anodic current, while the cathodic reaction provides oxygen ions according to Reaction (2) to form ZrO_2, resulting in the formation of the passive oxide film. O_o denotes an oxygen ion, and H_{bl} represents a hydrogen atom incorporated in the oxide barrier

layer [27]. OH^- can transport via imperfections, cracks or pores in the oxide film. Increasing the OH^- concentration accelerates the dissolution of zirconium oxide according to Reaction (3). OH^- had ~~a~~ less charge in comparison with O^{2-}, while both ions have a similar size [25]. Therefore, it is mainly OH^- instead of O^{2-} which diffuses through the oxide to the oxide/alloy interface when Zircaloy-4 is exposed in a LiOH aqueous solution. The anodic Tafel slope (β_a) decreases from 431.1 $mV \cdot dec^{-1}$ to 235.2 $mV \cdot dec^{-1}$ and the cathodic Tafel slope (β_c) increases from 154.2 $mV \cdot dec^{-1}$ to 306.8 $mV \cdot dec^{-1}$ when the concentration of LiOH in the aqueous solutions increases from 10 ppm to 10^4 ppm. More OH^- ions can transport the oxide film layer to form $HZrO_3^-$ with an increasing LiOH concentration according to Reaction (3), which facilitates the diffusion of products. Thus, the acceleration of the electrochemical corrosion anodic reaction results in the decrease of β_a and increased thickness of the oxide layer. This result contradicts the mass transfer process, which decelerates the cathodic reaction, resulting in the increase of β_c.

On the other hand, the lithium ion plays an important role in accelerating ~~the~~ corrosion. Kim [32] indicated that Li^+ can easily fit into the ZrO_2 crystal lattice due to its small size. In addition, the substitution of Li^+ for Zr^{4+} would produce excessive oxygen vacancies, which would in turn enhance the diffusion rate of O^{2-}. Thus, a higher concentration of LiOH provides more OH^- ions that can diffuse through the oxide film layer and react at an anion vacancy to form Zr-OLi groups. These Zr-OLi groups hinder the growth of ZrO_2, resulting in a decrease of the protective properties of the oxide barrier film. In summary, both OH^- and Li^+ facilitate the corrosion of Zircaloy-4 by weakening the passive, oxide barrier layer at its surface.

3.2. Electrochemical impedance spectroscopy

The EIS studies provide more information about the electrochemical behavior of the oxide film structure on the Zircaloy-4 surface. Fig. 2 and Fig. 3 show ~~the~~ Nyquist plots and Bode plots of the Zircaloy-4 in LiOH solution over a concentrations range from 10 to 10^4 ppm at 350°C and 16.5 MPa.

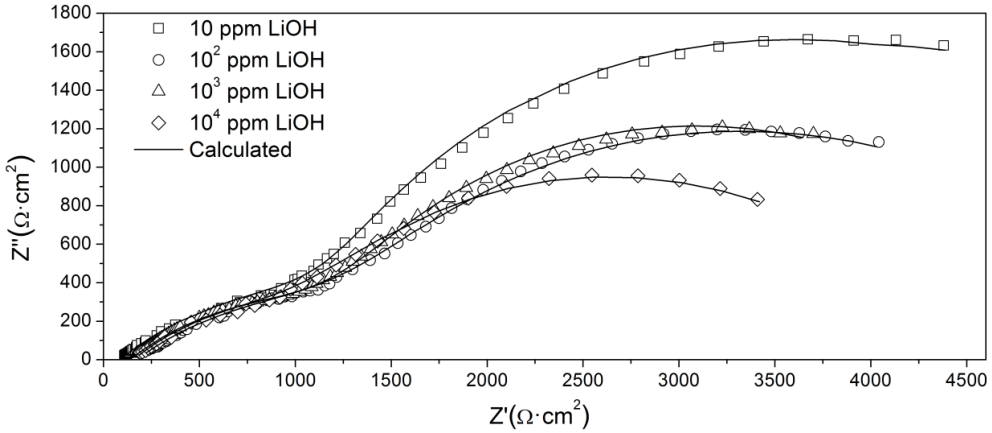

Figure 2. Nyquist plots for the oxide film form on Zircaloy-4 in LiOH solutions with different concentrations (350°C, 16.5 MPa)

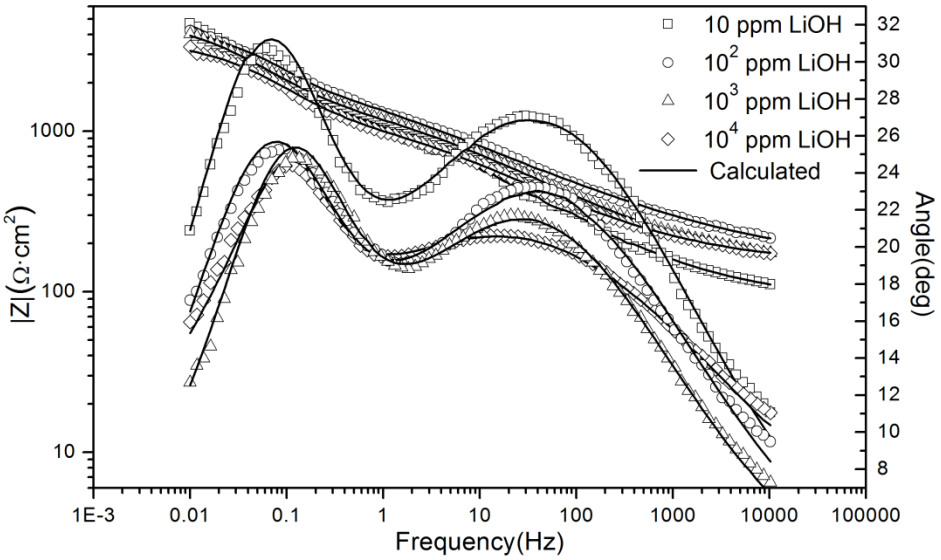

Figure 3. Bode plots for the oxide film form on Zircaloy-4 in LiOH solutions with different concentrations (350°C, 16.5 MPa)

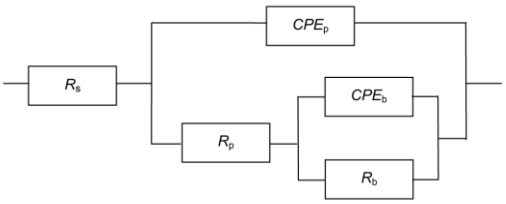

Figure 4. Equivalent circuit diagram for the oxide film form on Zircaloy-4 in LiOH solutions with different concentrations (350°C, 16.5 MPa)

Table 2. Impedance parameters of Zircaloy-4 in LiOH solution with different concentrations (350°C, 16.5 MPa)

C_{LiOH} (ppm)	CPE_p	n_p	R_p ($\Omega \cdot cm^2$)	CPE_b	n_b	R_b ($\Omega \cdot cm^2$)	Chi-Squared
10	2.31×10^{-4}	0.42	1972	7.67×10^{-4}	0.85	5180	1.01×10^{-4}
10^2	1.97×10^{-4}	0.41	1830	5.82×10^{-4}	0.72	4016	3.76×10^{-5}
10^3	2.03×10^{-4}	0.43	1679	8.03×10^{-4}	0.75	3783	1.52×10^{-5}
10^4	2.13×10^{-4}	0.45	1417	5.88×10^{-4}	0.70	3007	1.04×10^{-4}

The general features of these curves in Fig. 2 seem to be similar at all concentrations of LiOH with two capacitive loops in the measured frequency domain. In this study, the EIS plots with the

frequency range of 0.01–10,000 Hz show two time constants in Fig. 3, which are considered to fit the equivalent circuit shown in Fig. 4. The electrical circuit illustrates an oxide model that has two film layers, which has also been applied to explain the behavior of the double layer oxides on titanium or zirconium alloys [14, 33]. The capacitive loop in the high frequency range is attributed to the growth of the outer layer while the low frequency capacitive loop is related to the growth of the inner layer. A good fit of the data to this model was obtained and the fitting parameters are listed in Table 2.

In this equivalent electrical circuit, R_s refers to the solution resistance between the electrode and ~~the~~ electrolyte; CPE_p and R_p represent the capacitance element and resistance of the outer layer, while CPE_b and R_b represent the capacitance element and resistance of the inner layer respectively. It is noteworthy that constant phase elements (*CPE*) must be introduced to explain the deviation of the capacitances between the actual measurements and ~~the~~ ideal pure capacitances, due to the local inhomogeneities of the dielectric material, surface roughness and ~~the~~ relaxation effect, and ~~the~~ degree of deviation from the ideal capacitance depends on the value of $n(0<n<1)$ [34, 35].

It is observed that R_p decreases from 1972 Ω·cm² to 1417 Ω·cm² and R_b decreases from 5180 Ω·cm² to 3007 Ω·cm² when the concentration of LiOH in the aqueous solutions increases from 10 ppm to 10^4 ppm. These results indicate that increasing the LiOH concentration weakens the protective property of both the outer and ~~the~~ inner layers, promoting Zircaloy-4 corrosion. To analyze the reasons for this phenomenon, it is necessary to know the different formation mechanisms of the outer layer and inner layer. Parise et al. [36] reported that there was compressive stress in the oxide film during ~~the~~ zirconium oxide growth and the stress increased as the oxide layer becomes thickened. Using TEM, Park et al. [7] investigated the surface cracks on zirconium alloys after exposure to a LiOH solution and found a non-protective porous film resulting from internal stress relaxation. At the same time, the new protective oxide film formed at its surface was still dense, which can be regarded as the inner barrier film [37]. In this study, the results show that the value of n_b is approximately 0.8 and the value of n_p is approximately 0.4, indicating that the outer oxide layer is more porous. R_b is obviously bigger than R_p, suggesting the inner film has ~~a~~ better corrosion resistance ability. Due to the porosity of the outer oxide layer, Li^+ and OH^- can easily penetrate the film, causing R_p to decrease with the increasing LiOH concentration. As the oxide grows, the metal is transformed into ZrO_2, which entails an increase in volume of approximately 1.56 due to the Pilling-Bedworth ratio of the Zr/ZrO_2 system. There are high compressive stresses caused by the volume expander in the oxide film, and therefore, the ZrO_2 formed on the surface of the alloy exists crystal defects leading to the acceleration of electrochemical corrosion. Chen et al. [38] reported that ZrH_2 was produced at the barrier layer under simulated PWR situation via Reaction (4). In addition, Ai et al. [21] believed that ZrH_2 and OH^- ~~will~~l further reacted at the barrier layer (inner layer) / outer layer interface as Reaction (5). When the concentration of LiOH increases, the larger concentration of OH^- facilitates Reaction (5) and accelerates the dissolution of the barrier oxide film, thus decreasing R_b.

$$Zr + 2H_2O + 2e^- \rightarrow ZrH_2 + 2OH^- \quad (4)$$

$$ZrH_2 + 4OH^- \rightarrow ZrO^{2+} + 3H_2O + 6e^- \quad (5)$$

To summarize, the oxide film gradually forms at the oxide/metal interface, and becuase the oxygen ions have to pass the oxide film to reach the interface, ~~so~~ the oxide film performance ~~will~~ directly affects corrosion resistance. ~~And~~ OH^- can easily penetrate the outer layer oxide film to

dissolve the two-layer oxide, resulting in the acceleration of corrosion on Zircaloy-4. However, the potentiodynamic polarization and EIS results demonstrate that Zircaloy-4 shows excellent corrosion resistance in high-temperature and high-pressure LiOH solutions because of the presence of ~~the~~ alloyed elements such as Sn which stabilizes the formation of the quadratic phase. Sn is the element that stabilizes α and can form a substitute solid solution in the α and β phases. It has been reported that the corrosion resistance of the Zr-Sn alloys increased with increasing Sn content in LiOH solution [11].

Most previous studies studied the crystal structures of the oxide layers on ~~the~~ zirconium alloys by ex situ surface analysis after a long-term autoclave exposure, which were unable to illustrate the actual performance of the zirconium oxide in high-temperature and high-pressure aqueous solutions. By contrast, we can study the corrosion resistance ability of alloys by performing an electrochemical measurement over a short time. It is important to establish an in situ surface analysis technique to determine the microstructures in our future studies.

4. CONCLUSIONS

The electrochemical experimental results reveal that LiOH has an important effect on the corrosion behavior of Zircaloy-4 at 350°C and 16.5 MPa. The EIS and potentiodynamic polarization results demonstrate that the resistances of both the outer layer and ~~the~~ inner layer decrease when the concentration of LiOH increases and the electrochemical corrosion of Zircaloy-4 occurs more easily and faster at higher concentrations of LiOH due to the acceleration of the oxide film dissolution. Considering the above analysis, although Zircaloy-4 shows superior corrosion resistance in high-temperature and high-pressure aqueous solutions, LiOH still plays a detrimental role in the extreme simulated nuclear reactor environment. Therefore, ~~the~~ further research is needed on prolonging the service life of nuclear reactors in two ways: the first is to improve the anticorrosion ability by optimizing the zirconium alloy composition and the second ~~way~~ is to control the LiOH concentration by promoting the circulation of a water system in nuclear reactors.

ACKNOWLEDGMENTS
This work was financially supported by the National Key Research and Development Plan (2016YFC0600100), 135 Program of the Institute of Geochemistry, CAS, and Large-scale Scientific Apparatus Development Program (YZ200720), CAS.

References

1. A.M. Garde, *ASTM Stand. News*, 23 (1995) 28.
2. R. Krishnan, M.K. Asundi, *Proc. Indian Acad. Sci.*, 4 (1981) 41.
3. K. ABE, *J. Nucl. Sci. Technol.*, 28 (1991) 369.
4. B.G. Parfenov, *At. Energ.*, 42 (1977) 274.
5. A.Y. Rogozyanov, G.P. Kobylyansky, A.A. Nuzhdov, *J. ASTM Int.*, 5 (2008) 101105.
6. E. Hillner, *J. Electrochem. Soc.*, 3 (1967) 237.
7. J.Y. Park, S.J. Yoo, B.K. Choi, Y.H. Jeong, *J. Nucl. Mater.*, 373 (2008) 343.

8. J. Huang, M.Y. Yao, C.Y. Gao, P.F. Hu, X. Liang, J.L. Zhang, B.X. Zhou, Q. Li, E. Ahsan, *Corros. Sci.*, 104 (2016) 269.
9. M.Y. Yao, C.Y. Gao, J. Huang, J.C. Peng, X. Liang, J.L. Zhang, B.X. Zhou, Q. Li, *Corros. Sci.*, 100 (2015) 169.
10. J. Huang, M.Y. Yao, C.Y. Gao, X. Liang, J.C. Peng, J.L. Zhang, B.X. Zhou, *Corros. Sci.*, 99 (2015) 172.
11. Y.H. Jeong, J.H. Kim, H.G. Kim, *Met. and Mater. Int.*, 10 (2004) 453.
12. C. Daniel, R. Martin, F. Xavier, *Acta Mater.*, 87 (2015) 283.
13. B. Cox, C. Wu, *J. Nucl. Mater.*, 224 (1995) 169.
14. S.Y. Park, M.H. Lee, Y.H. Jeong, Y.H. Jung, *Met. and Mater. Int.*, 10 (2004) 541.
15. P. Barberis, A. Frichet, *J. Nucl. Mater.*, 273 (1999) 182.
16. O. Gebhardt, A. Hermann, *Electrochim. Acta*, 41 (1996) 1181.
17. M. Oskarsson, E. Ahlberg, K. Pettersson, *J. Nucl. Mater.*, 295 (2001) 97.
18. C. Bataillon, S. Brunet, *Electrochim. Acta*, 39 (1994) 455.
19. B. Cox, Y.M. Wong, *J. Nucl. Mater.*, 218 (1995) 324.
20. J. Ai, Y. Chen, M. Urquidi-Macdonald, D.D. Macdonald, *J. Electrochem. Soc.*, 154 (2007) C43.
21. J. Ai, Y. Chen, M. Urquidi-Macdonald, D.D. Macdonald, *J. Electrochem. Soc.*, 154 (2007) C52.
22. M. Bojinov, L. Hansson-Lyyra, P. Kinnunen, T. Saario, P. Sirkiä, *J. ASTM Int.*, 4 (2005) 183.
23. M. Bojinov, W. Cai, P. Kinnunen, T. Saario, *J. Nucl. Mater.*, 378 (2008) 45.
24. A.M. Al-Hashimi, *Key Eng. Mater.*, 20 (1991) 2443.
25. W.Q. Liu, B.X. Zhou, Q. Li, M.Y. Yao, *Corros. Sci.*, 47 (2005) 1855.
26. S. Müller, L. Lanzani, *J. Nucl. Mater.*, 439 (2013) 251.
27. M. Bojinov, V. Karastoyanov, P. Kinnunen, T. Saario, *Corros. Sci.*, 52 (2010) 54.
28. D.A. Palmer, M.L. Machesky, P. Bénézeth, D.J. Wesolowski, L.M. Anovitz, J.C. Deshon, *J. Solution Chem.*, 38 (2009) 907.
29. D.D. Macdonald, A.C. Scott, P. Wentrcek, *J. Electrochem. Soc.*, 126 (1979) 908.
30. S. Lin, H.P. Li, L.P. Xu, Y.Q. Zhang, C. Cui, *RSC Adv.*, 7 (2017) 33914.
31. A.J. Markworth, A. Sehgal, G.S. Frankel, *J. Electrochem. Soc.*, 146 (1999) 3672.
32. Y.S. Kim, S.C. Kwon, *J. Nucl. Mater.*, 270 (1999) 165.
33. J. Pan, D. Thierry, C. Leygraf, *Proc. Indian Acad. Sci.*, 41 (1996) 1143.
34. A.K. Jonscher, *Electrochim. Acta*, 35 (1990) 1595.
35. U. Rammelt, G. Reinhard, *Electrochim. Acta*, 35 (1990) 1045.
36. M. Parise, O. Sicardy, G. Cailletaud, *J. Nucl. Mater.*, 256 (1998) 35.
37. B. Yang, M.C. Li, M.Y. Yao, B.X. Zhou, J.N. Shen, *Acta Metall. Sin.*, 46 (2010) 946.
38. Y. Chen, M. Urquidi-Macdonald, D.D. Macdonald, *J. Nucl. Mater.*, 348 (2006) 133.